Model vs. Data based Approaches Applied to Fault Diagnosis in Drinking Water Transport Networks

M.À. Cugueró-Escofet[a,*], J. Quevedo[a], C. Alippi[b], M. Roveri[b], V. Puig[a], D. García[a], F. Trovò[b]

[a] *Supervision, Safety and Automatic Control research group, Polytechnic University of Catalonia, Gaia Research Bldg., 22 Rambla Sant Nebridi, 08222 Terrassa (Barcelona), Spain.*
[b] *Department of Electronics and Information, Politecnico di Milano, Piazza Leonardo da Vinci, 32 I-20133 Milano, Italy.*

Abstract

In this paper, the problem of fault diagnosis in drinking water transport networks (DWTNs) is addressed. Two different fault diagnosis approaches are proposed to deal with this problem. The first one is based on a model-based approach exploiting *a-priori* information regarding physical/temporal relations existing between the measured variables in the monitored system, providing fault detection and isolation capabilities by means of the residuals generated using these measured variables and their estimations. This *a-priori* information is provided by the topology and the physical relations between the elements constituting the system, which is used by design in order to derive fault diagnosis. Differently, the second approach does not require the physical *a-priori* information of the network to operate. It relies on a data-driven solution meant to exploit the spatial and temporal relationships present in the acquired data streams to detect and isolate faults. Relationships between data streams are modelled through sequences of linear dynamic time-invariant models whose estimated coefficients are used to feed a Hidden Markov Model (HMM). When the pattern of estimated coefficients cannot be explained by the trained HMM, a change is detected. Afterwards, a cognitive method based on a functional graph representation of the system isolates the fault. Finally, a performance comparison between these two approaches is carried out using a part of the Barcelona water transport network.

[*] Corresponding author
Email address: miquel.angel.cuguero@upc.edu (M.À. Cugueró-Escofet)

Keywords: Fault isolation, cognitive systems, model-based fault diagnosis, time series, hidden Markov models, critical infrastructure systems

1. Introduction

Water networks are complex large-scale systems needing highly sophisticated supervisory and control schemes to satisfy a certain degree of performance when unfavorable faulty conditions are occurring. To deal with this problem, the use of a Fault Detection and Isolation (FDI) system capable to detect and isolate these faults (or events) is highly desirable, aiming to help the operators to identify which is the actual event occurring in the water network. The FDI problem applied to water networks has been extensively studied from various perspectives and at different levels (see, e.g. Colombo and Karney, 2002; Misiunas et al., 2006; Lees, 2000). On the one hand, at the District Metering Area (DMA) level, many FDI approaches have addressed the problem of leak/burst detection and isolation (see, e.g. Wu et al., 2010; Perez et al., 2011; Bicik et al., 2011; Mounce et al., 2009; Mounce and Boxall, 2010; Mounce et al., 2011; Romano et al., 2013, 2014a,b; Palau et al., 2011), where different model-based approaches are applied. Sensor data validation and reconstruction when exploiting the temporal redundancy of the sensor measurements is also addressed in several works (see, e.g. Quevedo et al., 2010; Eliades and Polycarpou, 2012; Prescott and Ulanicki, 2001; Filion et al., 2007; Farley et al., 2012). The problem of water quality monitoring concerning contamination event detection has also been extensively addressed (see, e.g. Eliades and Polycarpou, 2010). Moreover, regarding DMA monitoring (either for leaks or quality) there is a related problem considering optimal sensor placement in order to maximise the performance of the FDI algorithms applied. This problem has been studied separately both for leak detection and location (see, e.g. Casillas et al., 2014; Pérez et al., 2010; Krause et al., 2008; Wu, 2011; Ostfeld and Salomons, 2004) and quality monitoring (see, e.g. Eliades and Polycarpou, 2010). On the other hand, at the water transportation level (i.e. the network connecting the water potabilisation plants with the water distribution tanks) less research has been carried out (see, e.g., Ragot and Maquin, 2006; Quevedo et al., 2014). The water transportation networks,

also referred to as trunk main systems, are regional networks used to supply water to the cities and villages of a certain region. This kind of networks can be analysed using a flow-driven model, that is, using mass-balance linear relations, alternatively to water distribution networks, which are generally modelled using pressure-driven models implying non-linear non-explicit relations. The use of mass balance relations for modelling regional water transport networks is appropriate because an actuator is typically installed in each pipe, which establishes its flow. Of course, the energy balances could also be formulated in this case, but this would add extra complexity which is actually not needed since the goal is to establish analytical redundancy relations between flow sensors. This is the case e.g. in Quevedo et al. (2014), where the problem of sensor data validation and reconstruction (which is addressed for DMA networks in Quevedo et al. (2010) exploiting the temporal redundancy of the sensor measurements) has been extended to transport water networks, considering combined temporal/spatial redundancy models. In Ragot and Maquin (2006), a model-based FDI approach is applied to the Nancy water network, a city in the north-eastern French department of *Meurthe-et-Moselle*, in order to detect faults in the sensors. The present paper also goes towards the FDI application to a water transport network by proposing two different fault diagnosis approaches: a model-based approach using *a-priori* information of the system, i.e. the physical relation between its elements, and a data-driven approach, which is able to exploit *a-priori* information about the network topology to perform fault diagnosis but does not require any additional information about the physical models of the water transport network. According to the literature, model-based approaches rely on the concept of analytical redundancy (Blanke et al., 2006), which is based on the use of software sensors i.e. models using available sensor historic records in order to estimate the desired sensor measurement, as an alternative to hardware-based approaches, which rely on the use of extra hardware sensors. Although hardware redundancy is desirable in critical elements, the use of the latter in large-scale water networks may be dramatically expensive because of the installation, calibration and maintenance actions to be performed on the system when considering this approach.

The novelty in this paper is to address the fault diagnosis problem in drinking water transport networks (DWTNs) by applying and comparing two well accepted gen-

eral purpose fault diagnosis methods (one model-based, the other data-based). The Barcelona DWTN is used as the case study in this work. In ideal situations, the use of a model obtained from the physical relations, as considered in the first approach, should lead to the optimal solution. However, it may be noted that analytical models may be affected by several system practical aspects, such as the potential uncertainty on the model parameters (e.g. actual tank surface), the difficulty to have an on-line well-calibrated model due to frequent network topology changes (caused by e.g., new elements like tanks added or blocked pipes resulting from maintenance operations) and common changes on the consumers demand behavior, which are hard to determine in real-time operation. Hence, a data-based approach, as suggested in the second method, is also a useful and effective alternative to the use of analytical models obtained from physical/temporal relations existing in the network.

The structure of the paper is as follows: Section 2 shows the Barcelona DWTN. Section 3.1 presents an FDI model-based method combining both spatial and time series models, whilst Section 3.2 presents the data based approach based on a Cognitive Fault Diagnosis System (CFDS) method exploiting Hidden Markov Models (HMMs). In Section 4, fault isolation results obtained by each methodology are presented, compared and discussed. Finally, conclusions and on-going work are outlined in Section 5.

2. Case study: Barcelona Drinking Water Transport Network

The Barcelona DWTN (Figure 1), considered as a case study here, is distributed in 23 different districts covering 424 Km^2 area and providing water to about three million end users. Water managed by this transport network is obtained from both surface and underground sources, including Ter (surface source) and Llobregat (both surface and underground source) as the most important ones in terms of usage and capacity. The water supplied by these sources is distributed through a network of around 4645 Km of pipes to 218 District Metered Areas or demand sectors (DMAs), including about 400 controlled/monitored points, 63 storage tanks, 84 pumps, 46 valves and 88 pressure floors. Transport networks are constituted by multiple similar tank subsystems which have alike behavior. In this work, the analysis of a single tank subsystem and a three-

tank subsystem is considered (*Orioles* and *Can Guey* in Figure 1 and Figures 6 and 7, respectively). Similar results are also achieved when considering alternative tank subsystems in the same DWTN. Regarding data management, the Barcelona telecontrol system receives real-time data mainly from the available flow meters, usually installed in the DMAs supply points, so their reading closely fit the actual DMAs water demand.

3. Fault Diagnosis Methodology

In this work, two different well accepted general purpose fault diagnosis methodologies are used to address the FDI problem in DWTNs. The first approach is based on checking the consistency between the observed and the nominal system behavior by means of a set of Physical/Temporal Parity Relations (PTPR), which relates the measured system variables under normal (faultless) operation assumption of the monitored system. The novelty of the PTPR approach presented here relies on the combined usage of time series residuals with physical residuals, by means of a classical FDI residual-based approach which generally considers only physical parity relations. An inconsistency is detected when analytical redundancy relations derived from models do not match the measurements, generating a non-null residual. Then, the fault diagnosis mechanism is activated in order to isolate the possible fault by matching the residuals against the fault signature matrix (see, e.g. Puig et al. (2006)). The proposed FDI scheme is shown in Figure 2, where $u_i(k)$ is the i-th measured system input, $x_i(k)$ is the i-th measured system output, $\hat{x}_i(k)$ is the i-th predicted system output, $r_i(k)$ is the i-th system residual of the complete set of n_r residuals and $\mathbf{s}(k)$ is the corresponding fault signature at time instant k. Further details on this general fault diagnosis scheme are given later in this section.

The second approach relies on the CFDS method presented in Alippi et al. (2013), that is able to exploit spatial and temporal relationships among measured system variables. The considered CFDS, which does not require any *a-priori* information about the physical model of the network, is based on a two-layer hierarchical architecture to detect and isolate faults. In the first layer, a change-detection test (CDT) based on HMMs (see, e.g. Alippi et al. (2012)) is able to detect a fault occurring in the system

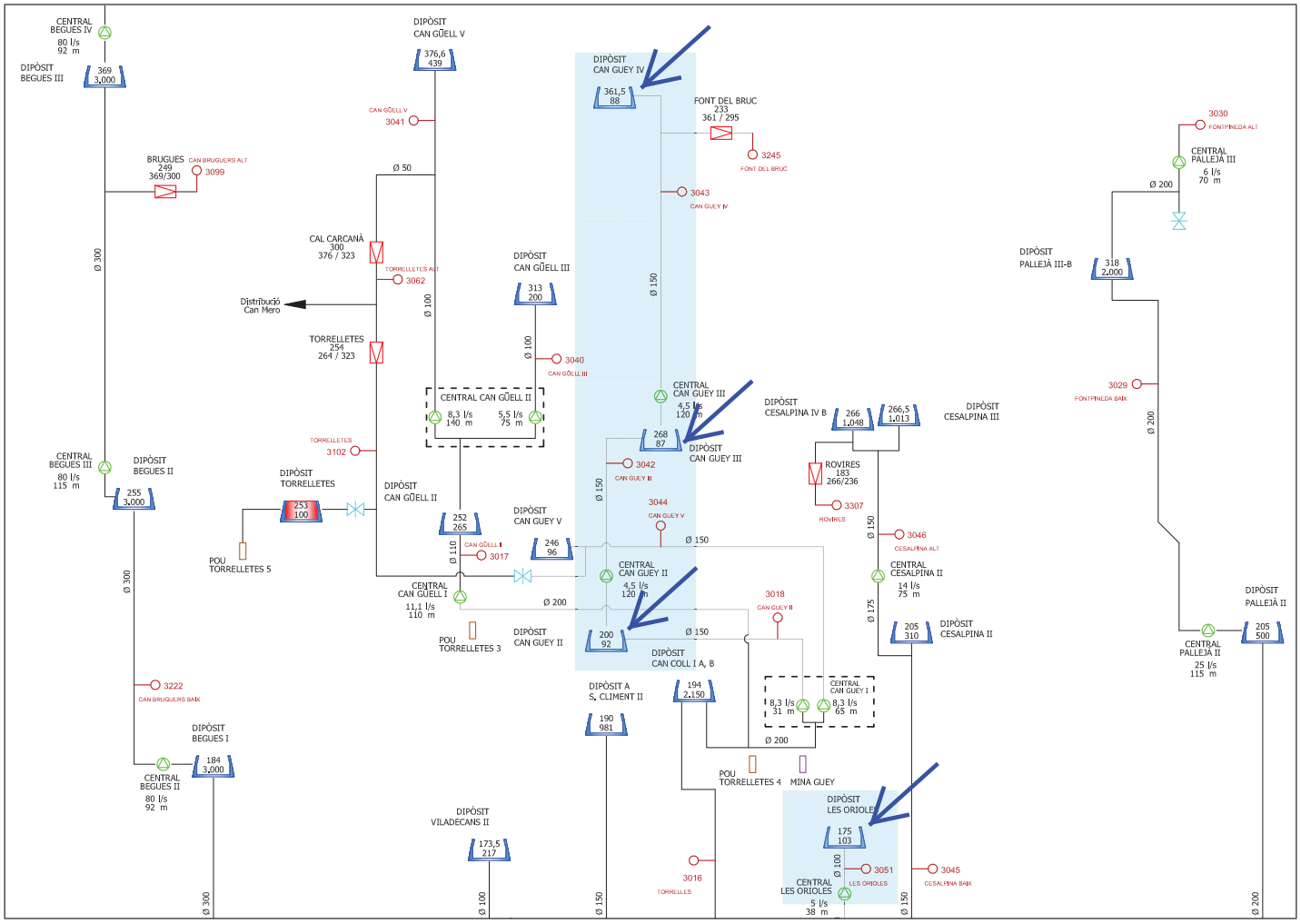

Figure 1: Barcelona Drinking Water Transport Network (DWTN) detail, including Orioles and Can Guey subsystems (arrows)

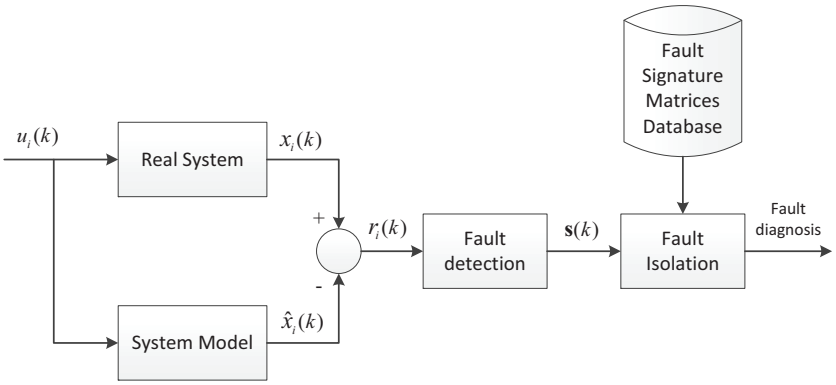

Figure 2: Fault Detection and Isolation (FDI) block diagram

by checking the variations in the relationship between couples of data streams, while, in the second layer, a cognitive method based on a functional graph representation of the system is able to isolate the fault occurring. Here, we are proposing a modified version of the original CFDS, specifically crafted for this application, where the available topological information of the water network is integrated into the data-driven approach. For instance, Figure 3(a) represents all the relationships which may exists among data coming from the *Can Guey* subsystem (Figure 7) induced by the water flow physical phenomenon. This initial dependency graph in Figure 3(a) is reduced by taking into account the correlation analysis and the final outcome of the *Can Guey* subsystem (Figure 3(b)).

3.1. Method I: Fault diagnosis based on Physical/Temporal Parity Relations

3.1.1. Residual generation

The fault diagnosis method presented in this section evaluates the nominal residual $r_i(k)$ obtained from the difference between the system measurements and the model prediction, considering the model for the i-th subsystem expressed in input-output regressor form as follows

$$r_i(k) = x_i(k) - \hat{x}_i(k) = x_i(k) - \phi_i^T(k)\theta_i \tag{1}$$

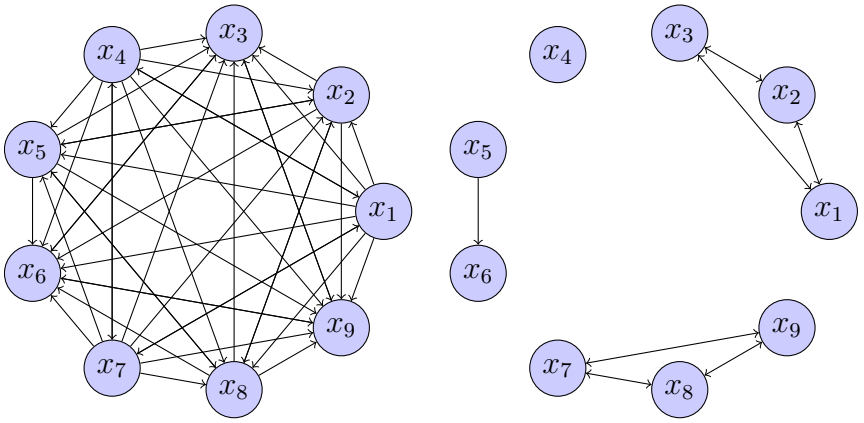

(a) Complete (b) Reduced

Figure 3: CFDS method dependency graphs of *Can Guey*

where θ_i are the nominal parameters obtained using a training dataset, $x_i(k), i \in \{1, \ldots, N\}$ is the sensor measurement at time instant k, $N \in \mathbb{N}$ is the number of considered sensors, $\hat{x}_i(k)$ is the model prediction at time instant k and $\phi_i(k)$ is the regressor vector of dimensions $n_{\theta_i} \times 1$, including inputs $(u_i(k), u_i(k-1), u_i(k-2), ...)$ and outputs $(y_i(k), y_i(k-1), y_i(k-2), ...)$. Considering the uncertainty (e.g. modelling errors, noise) the detection test involves checking the condition

$$|r_i(k)| < \tau_i(\mu_i, \sigma_i) \tag{2}$$

where τ_i is the detection threshold, which is function of the mean value μ_i and the standard deviation σ_i of the i-th residual (i.e. $\tau_i = \mu_i + 3\sigma_i$, including the 99.7 % of the values of a normal distribution according to the *3-sigma* rule) which, according to the central limit theorem, is assumed to follow a Gaussian distribution. The threshold in (2) is designed to include the values of the whole residual distribution in the faultless situation and hence, it may be used for fault detection purposes. Test condition (2) can be equivalently expressed as follows:

$$x_i(k) \in [\underline{\hat{x}}_i(k), \bar{\hat{x}}_i(k)] \tag{3}$$

where $\bar{\hat{x}}_i(k) = \hat{x}_i(k) + \tau_i$ and $\underline{\hat{x}}_i(k) = \hat{x}_i(k) - \tau_i$, respectively.

Spatial consistency residuals. The PTPR method is based on establishing mass balance equations for the water network constitutive elements. As an example, the mass balance expression for the i-th tank can be stated by means of the following discrete-time difference equation

$$y_i(k+1) = y_i(k) + \frac{\Delta t}{A_i}\left(q_{in_i}(k) - q_{out_i}(k)\right) \tag{4}$$

where $y_i(k)$ is the tank level, A_i is the cylindrical tank surface, $q_{in_i}(k)$ is the manipulated inflow and $q_{out_i}(k)$ is the outflow, which may include manipulated tank outflow and consumer demands, both given in m^3/s.

Similarly, in the water transport network nodes, the mass balance may be expressed as the static equation

$$\sum_i q_{in_i}(k) = \sum_i q_{out_i}(k) \tag{5}$$

where, similarly to Equation (4), $q_{in_i}(k)$ and $q_{out_i}(k)$ correspond to the inflow and outflow of the i-th subnet node, also given in m^3/s.

Time series residuals. Additional residuals can be obtained considering that level in tanks and flow in demand sectors have a daily repetitive behavior which can be modelled using a Time Series (TS) model. TS models take advantage of the temporal redundancy of the measured variables. A wide used method for signal forecasting is the Holt Winters (HW) triple exponential smoothing approach (Winters, 1960; Makridakis et al., 1998). This method, which is of wide use because of its simplicity and performance, may be presented in several different versions e.g. additive or damped trend, additive or multiplicative seasonality, single or multiple seasonality. Here the additive single seasonality version is considered, which may be implemented as shown next for a forecasting horizon ℓ

$$\hat{x}_{ts}(k) = \hat{R}(k-\ell) + \ell\hat{G}(k-\ell) + \hat{S}(k-L) \tag{6}$$

where $\hat{x}_{ts}(k)$ is the TS model forecasted value, $\hat{R}$ is the estimate of the deseasonalized level (i.e. removing the seasonal effect $\hat{S}(k - L - \ell)$), $\hat{G}$ is the estimate of the trend and $\hat{S}$ is the estimate of the seasonal component, which may be respectively stated as follows

$$\begin{aligned}\hat{R}(k-\ell) =& \alpha\left(x(k-\ell) - \hat{S}(k-\ell-L)\right) \\ &+ (1-\alpha)\left(\hat{R}(k-\ell-1)\right. \\ &\left.+\hat{G}(k-\ell-1)\right) \quad 0<\alpha<1\end{aligned} \tag{7}$$

$$\begin{aligned}\hat{G}(k-\ell) =& \beta\left(\hat{R}(k-\ell) - \hat{R}(k-\ell-1)\right) \\ &+ (1-\beta)\,\hat{G}(k-\ell-1) \quad 0<\beta<1\end{aligned} \tag{8}$$

$$\begin{aligned}\hat{S}(k-\ell) =& \gamma\left(x(k-\ell) - \hat{R}(k-\ell)\right) \\ &+ (1-\gamma)\,\hat{S}(k-\ell-L) \quad 0<\gamma<1\end{aligned} \tag{9}$$

where L is the season (i.e. daily here) periodicity, α, β and γ are the HW parameters (level, trend and season smoothing factors, respectively) and x is the measured value (i.e. y_m, q_{in_m} or q_{out_m}, depending on the TS model considered). Hence, analysing the historic records of the measured values in a certain sensor, a HW model is derived and used to validate the current data acquired by this device.

3.1.2. FDI scheme

The FDI methodology (Figure 2) is based on determining the *actual fault signature* $\mathbf{s}(k) = [s_1(k), s_2(k), \ldots s_{n_r}(k)]$ of the system for n_r different residuals, as a result of the fault detection phase (see Section 3.1.1) as follows

$$s_i(k) = \begin{cases} 0, & \text{if } |r_i(k)| < \tau_i \text{ (no fault)} \\ 1, & \text{if } |r_i(k)| \geq \tau_i \text{ (fault)} \end{cases} \tag{10}$$

where τ_i is the threshold associated to the i-th residual. The actual fault signature is compared against the *theoretical Fault Signature Matrix* (FSM) Σ that binary codifies the influence of each fault in the set of considered faults $f_1, f_2, \ldots f_{n_f}$ on every residual in the set of considered residuals $r_1, r_2, \ldots r_{n_r}$. This matrix has as many rows as residuals and as many columns as considered faults. If $\Sigma_{ij} = 1$, the j-th fault appears in the expression of the i-th residual; otherwise $\Sigma_{ij} = 0$. Assuming classical FDI fault hypotheses, i.e, single faults and no-compensation (exoneration), fault isolation consists in looking for a column of Σ matching the actual fault signature $\mathbf{s}(k)$. More details about the algorithm implementation of this FDI scheme, including how to manage the temporal aspects of the binarized residuals, can be found in Meseguer et al. (2010) and Puig and Blesa (2013).

3.2. Method II: Fault Diagnosis System based on the Cognitive Approach

The considered CFDS method is based on the ability to characterize the functional dependencies among the streams of acquired data, where each functional dependency models the temporal and spatial relationships between couples of data streams. The main characteristics of the CFDS are the ability to work without any *a-priori* information about the physical models of the system and the possibility to isolate the potential faults by exploiting a functional graph representation of the system. Details about the considered CFDS can be found in Alippi et al. (2013). In this applicative scenario, we considered the possibility to include the *a-priori* information about the topology of the water transport network. In fact, the physical phenomenon of the water flow induces a causality among the respective acquired data streams, allowing to discard those relationships in which this causality principle does not hold.

The overall system architecture is presented in Figure 4. Each relationship is evaluated over time using a HMM-based CDT aiming to analyse the statistical behaviour of the estimated functional-relationship parameters over time. When a change in the estimated parameters is detected, the CFDS layer is activated to isolate the fault occurring in the system.

In more detail, let x_i be the i-th stream over the N sources of data within the considered sensors network. Let $g_{(i,j)}, i, j \in \{1, \ldots, N\}$ be the functional relationship (in

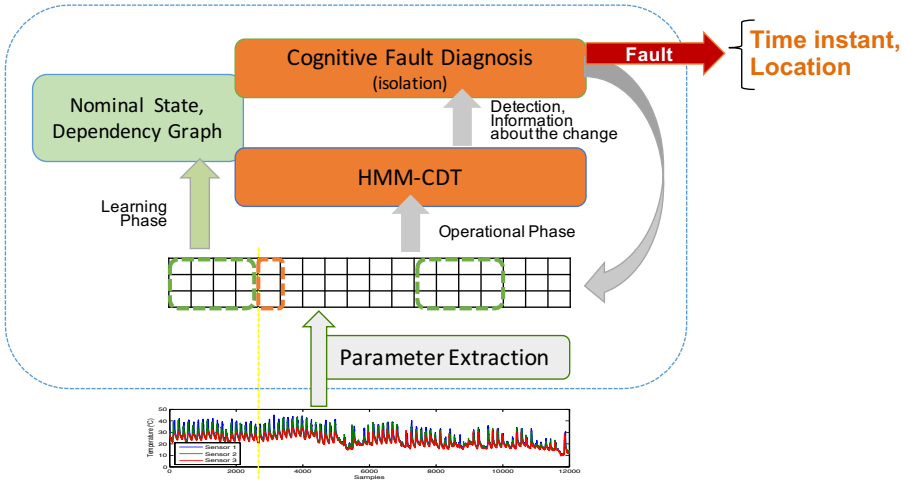

Figure 4: General architecture of the considered CFDS method

terms of transfer function) between the i-th and the j-th sensor. All the functional relationships present in the acquired data can be modelled as a *Dependency Graph* $\mathcal{G}$, where the nodes of this graph represent the N sensors of the network, while the arcs between nodes represent the functional relationships. We emphasize that generally, in real-world situations, not all the relationships are meaningful, since there might be nonexistent or very weak relationships between two streams of data. To address this issue, we only consider those relationships not contradicting the causality provided by the physical phenomenon and, subsequently, we resort to the use of the analysis of the linear correlation between x_i and x_j to define a level of dependency associated with $g_{(i,j)}$. More specifically, to remove weakly correlated streams of data, those data streams with cross-correlation peak absolute value below a certain threshold $\xi_{\min}$, with $0 \leq \xi_{\min} \leq 1$, have been removed (e.g. $\xi_{\min}$ can be set to 0.5 or larger, depending on the network complexity, to keep only highly correlated data streams). This led to the definition of a *reduced dependency graph* $G = \{V, E\}$, where V and E are the set of nodes representing the N network sensors and the set of arcs representing relationships characterized by higher correlation (i.e. cross-correlation above $\xi_{\min}$), respectively. Figures 3(b) and 5 show examples of the reduced dependency graph for Can Guey and

Orioles systems, respectively.

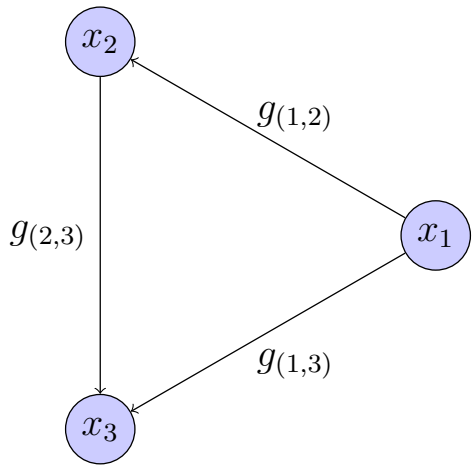

Figure 5: Example of a reduced dependency graph with three sensors (i.e., x_1, x_2 and x_3) and three relationships (i.e., $g_{(1,2)}$, $g_{(1,3)}$ and $g_{(2,3)}$).

Functional relationships $g_{(i,j)}$ in G are modelled either by a linear time-invariant (LTI) dynamic system or by a sequence of LTI dynamic systems following the HMM hypothesis (i.e., the Markov memoryless property of stochastic processes). Among the wide range of LTI dynamic systems, we focus on Single-Input Single-Output (SISO) models such as AutoRegressive with eXogenous input (ARX) models, AutoRegressive Moving Average with eXogenous inputs (ARMAX) models or Output Error (OE) models (Ljung, 1999) in their predictive form, i.e., $g^{\theta}_{(i,j)}$ parametrized in $\theta \in \mathbb{R}^p$. Here, θ represents parameter vector of the considered predictive models, while p represents the cardinality of θ.

Assuming that the data generating process satisfies the exponential stability for closed loop and following the hypotheses on $g^{\theta}_{(i,j)}$ stated in (Ljung, 1978), the theoretical results in (Ljung, 1978) grant that

$$\sqrt{N_T} P^{-\frac{1}{2}} (\hat{\theta} - \theta^*) \sim \mathcal{N}(0, I_p) \quad \text{when } N_T \to \infty, \tag{11}$$

where $P \in \mathbb{R}^{p \times p}$ is the covariance matrix of the estimated parameter $\hat{\theta}$ of the model, N_T is the length of the training set used to estimate $\hat{\theta}$ with the Least Square (LS) method,

θ^* is the optimal configuration of the parameters within the chosen model family and I_p is the identity matrix. From Eq. (11) it may be stated that, given N_T sufficiently large, the distribution of the estimates $\hat{\theta}$s follows a multivariate Gaussian with mean vector θ^* and covariance matrix P. This theoretical result led us to consider HMMs ruled by a mixture of Gaussians (GMM) to model the statistical behaviour of estimated parameters $\hat{\theta}$ over time. In more detail, the HMM is defined as

$$\mathcal{H} = \{n, \mathcal{F}, A, \pi\}, \tag{12}$$

where n is the number of states, $\mathcal{F} = \{p_1, \ldots, p_n\}$ is the set of Probability Density Functions (PDFs) associated with each state, $A \in [0,1]^{n \times n}$ is the state transition probability matrix and $\pi \in [0,1]^n$ is the initial state distribution vector. It is worth noting that Eq. (11) allows us to model the PDF associated with the nominal state by using a GMM. Let

$$p_i(\hat{\theta}|\Phi_i) = \sum_{k=1}^{K_i} w_{k,i} \mathcal{N}(\hat{\theta}|\mu_{k,i}, \Sigma_{k,i}) \tag{13}$$

be the GMM associated with the i-th state, where K_i is the number of Gaussian mixtures for the i-th state, $w_{k,i}$ is the weight for state i and Gaussian mixture k,

$$\Phi_i = [\mu_{1,i}, \ldots, \mu_{k_i,i}, \Sigma_{1,i}, \ldots, \Sigma_{k_i,i}] \tag{14}$$

with $\mu_{k,i}$ and $\Sigma_{k,i}$ the mean vector and the covariance matrix for state i and Gaussian mixture k, respectively.

The analysis of the evolution over time of estimated parameters $\hat{\theta}$s by means of a HMM is the core mechanism of the HMM-based CDT. More specifically, for each $g_{(i,j)} \in V$, the sequence of $\hat{\theta}$s are estimated by overlapping windows of N_T observations. The HMM $\mathcal{H}_{(i,j)}$, associated to relationship $g_{(i,j)}$, is trained on the estimated parameters computed from the first T_0 observations, i.e., the training dataset. Then, after the training phase, the HMM-based CDT keeps on estimating the parameter $\hat{\theta}$ by overlapping windows of data, and let $\hat{\theta}^s$ be the parameter estimated on the s-th window. The log-likelihood of the HMM is as follows

$$l_{(i,j)}(s) = P(\hat{\theta}^{s-\omega+1}, \ldots, \hat{\theta}^{s} | \mathcal{H}_{(i,j)}) \tag{15}$$

where ω is the considered log-likelihood window length. This value indicates how likely the sequence of parameters $\hat{\theta}^{s-\omega+1}, \ldots, \hat{\theta}^{s}$ has been generated by $\mathcal{H}_{(i,j)}$. When $l_{(i,j)}$ decreases below an automatically defined threshold (i.e., the minimum value assumed by the log-likelihood in training or validation scaled by a user-defined coefficient factor), a change in the relationship $g_{(i,j)}$ is detected. Details about the HMM-based CDT can be found in Algorithm 1 of Alippi et al. (2013) and in Alippi et al. (2012).

Once a change in one of the HMM-based CDTs is detected, the Cognitive Fault Diagnosis layer is activated to isolate the fault within the system. The basic idea of this cognitive isolation mechanisms is as follows: when a fault affects a sensor, all the relationships connected to that sensor should be affected by this change. Hence, by looking at the likelihood of all the relationships in V, we are able to identify the sensor of the system that has been affected by the fault, and thus to isolate it. Details about the cognitive level presented here can be also found in Algorithm 2 of Alippi et al. (2013).

4. Experimental Results

In this paper, the two fault diagnosis methods introduced in previous section are tested using a simulator of the Barcelona DWTN. This simulator is developed under MATLAB/SIMULINK platform, using a model calibrated and validated with real data which provides a good representation of the actual water network behavior. Without loss of generality, the results presented here are focused on two subsystems within the Barcelona water transport network (Figure 1), known as Orioles (Figure 6) and Can Guey (Figure 7), in order to illustrate the performance of the fault diagnosis methodologies presented. This part of the network includes the following elements:

- **Tanks:** *d175LOR, d200CGY, d268CGY, d361CGY*
- **Actuators with flow sensors:** *iOrioles, iCanGuey1d2, iCanGuey2, iCanGuey3*
- **Demands with flow sensors:** *c175LOR, c200CGY, c268CGY, c361CGY*
- **Level sensors:** *xd175LOR, xd200CGY, xd268CGY, xd361CGY*

4.1. Residual Definition

In Figure 6 and Figure 7, q_{in}, q_{out} and y are the incoming tank flow, consumer demand and tank level, respectively, and q_{in_m}, q_{out_m} and y_m are the corresponding measured values. The corresponding discrete-time model equations, including the considered faults, are as follows

- Tank (level):

$$y(k+1) = y(k) + \frac{\Delta t}{A}\left[q_{in}(k) - q_{out}(k)\right] \tag{16}$$

- Pump (flow):

$$q_{in}(k) = \Gamma_p(k) q_p(k) + f_p(k) \tag{17}$$

- Tank level sensor:

$$y_m(k) = \Gamma_{y_m}(k) y(k) + f_{y_m}(k) \tag{18}$$

- Pump flow sensor:

$$q_{in_m}(k) = \Gamma_{q_{in_m}}(k) q_{in}(k) + f_{q_{in_m}}(k) \tag{19}$$

- Demand sector flow sensor:

$$q_{out_m}(k) = \Gamma_{q_{out_m}}(k) q_{out}(k) + f_{q_{out_m}}(k) \tag{20}$$

where $y(k)$ is the actual tank level, $y_m(k)$ is the measured tank level, $q_{out}(k)$ is the actual demand flow, $q_{out_m}(k)$ is the measured demand flow, $q_{in}(k)$ is the actual input tank flow, $q_p(k)$ is the set-point pump flow, $q_{in_m}(k)$ is the measured input flow, $\Gamma_c(k)$ is the multiplicative fault signal component related to element c, $f_c(k) = \beta_c(k)\chi_c(k)$ is the additive fault signal component related to element c, with $\beta(k)$ time profile and $\chi(k)$ behavior, Δt is the sampling time and A is the cylindrical tank surface.

Spatial consistency residuals can be obtained using the mass flow model (16) and the sensor measurements (17)-(20) in a non-faulty situation. In particular, the following

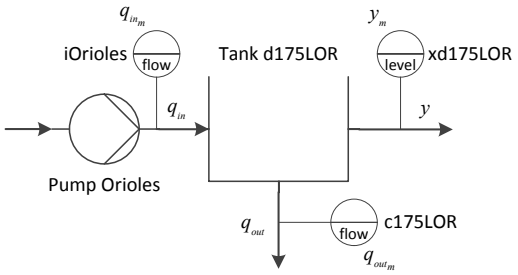

Figure 6: Orioles subsystem

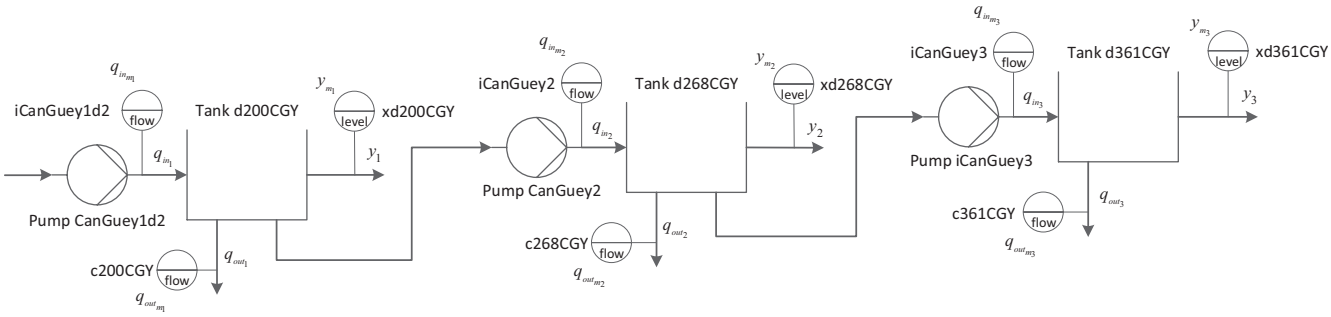

Figure 7: Can Guey subsystem

residual $r_{i,1}$ may be obtained using the tank model (16) for the i-th tank subsystem using measured variables

$$r_{i,1}(k) = y_{m_i}(k) - \hat{y}_{sc_i}(k) \tag{21}$$

with

$$\hat{y}_{sc_i}(k) = y_{m_i}(k-1) + \frac{\Delta t}{A_i}\left[q_{in_{m_i}}(k-1) - q_{out_{m_i}}(k-1)\right] \tag{22}$$

where $\hat{y}_{sc_i}$ is the tank level spatial consistency estimation, A_i is the cylindrical tank surface, $q_{in_{m_i}}$ is the manipulated measured inflow and $q_{out_{m_i}}$ is the measured outflow, both given in m^3/s.

Furthermore, for each input and output with periodic behaviour of the i-th tank subsystem, a TS HW model can be derived and the following Analytical Redundancy

Relations (ARRs) may be obtained:

- Tank (level) TS:

$$\hat{y}_{ts_i}(k) = g(y_{m_i}(k-1), ..., y_{m_i}(k-L)) \tag{23}$$

- Demand sector flow TS:

$$\hat{q}_{out_{ts_i}}(k) = h(q_{out_{m_i}}(k-1), ..., q_{out_{m_i}}(k-L)) \tag{24}$$

- Pump flow TS:

$$\hat{q}_{in_{ts_i}}(k) = l(q_{in_{m_i}}(k-1), ..., q_{in_{m_i}}(k-L)) \tag{25}$$

where g, h and l are the HW TS expressions (6)-(9) for the tank level sensor, sector demand sensor and pump flow sensor respectively, for data exhibiting a periodicity of L samples.

Using the TS models (23)-(25), the following residuals are obtained

$$r_{i,2}(k) = y_{m_i}(k) - \hat{y}_{ts_i}(k) \tag{26}$$

$$r_{i,3}(k) = q_{out_{m_i}}(k) - \hat{q}_{out_{ts_i}}(k) \tag{27}$$

$$r_{i,4}(k) = q_{in_{m_i}}(k) - \hat{q}_{in_{ts_i}}(k) \tag{28}$$

It may be noted that TS residuals in Equations (26)-(28) can only be applied for those sensors presenting periodic behavior. This is applicable to all the faulty elements considered in this work and also to the major part of the elements of the network, but still there are some which are not expected to evolve periodically (e.g. pump stations not directly serving water to a demand sector). Hence, in order to apply PTPR fault isolation methodology using TS residuals, elements involved should be previously checked for periodic behavior. As a counterpart, TS residuals may be computed with information provided by a single sensor, which may be advantageous in certain applications with non-obvious/non-existent model relation among sensors, e.g. intelligent sensors with embedded diagnosis unit (Alippi et al. (2012)).

Table 1: Faults signatures

	f_{y_m}	$f_{q_{out_m}}$	$f_{q_{in_m}}$	f_p	$f_{y_{m1}}$	$f_{q_{out_{m1}}}$	$f_{q_{in_{m1}}}$	f_{p1}	$f_{y_{m2}}$	$f_{q_{out_{m2}}}$	$f_{q_{in_{m2}}}$	f_{p2}	$f_{y_{m3}}$	$f_{q_{out_{m3}}}$	$f_{q_{in_{m3}}}$	f_{p3}
$r_{1,1}$	1	1	1	1	0	0	0	0	0	0	0	0	0	0	0	0
$r_{1,2}$	1	0	0	1	0	0	0	0	0	0	0	0	0	0	0	0
$r_{1,3}$	0	1	0	0	0	0	0	0	0	0	0	0	0	0	0	0
$r_{1,4}$	0	0	1	1	0	0	0	0	0	0	0	0	0	0	0	0
$r_{2,1}$	0	0	0	0	1	1	1	1	0	0	0	0	0	0	0	0
$r_{2,2}$	0	0	0	0	1	0	0	1	0	0	0	0	0	0	0	0
$r_{2,3}$	0	0	0	0	0	1	0	0	0	0	0	0	0	0	0	0
$r_{2,4}$	0	0	0	0	0	0	1	1	0	0	0	0	0	0	0	0
$r_{3,1}$	0	0	0	0	0	0	0	0	1	1	1	1	0	0	0	0
$r_{3,2}$	0	0	0	0	0	0	0	0	1	0	0	1	0	0	0	0
$r_{3,3}$	0	0	0	0	0	0	0	0	0	1	0	0	0	0	0	0
$r_{3,4}$	0	0	0	0	0	0	0	0	0	0	1	1	0	0	0	0
$r_{4,1}$	0	0	0	0	0	0	0	0	0	0	0	0	1	1	1	1
$r_{4,2}$	0	0	0	0	0	0	0	0	0	0	0	0	1	0	0	1
$r_{4,3}$	0	0	0	0	0	0	0	0	0	0	0	0	0	1	0	0
$r_{4,4}$	0	0	0	0	0	0	0	0	0	0	0	0	0	0	1	1

From residuals (21), (26) to (28) and equations (17) to (20) the theoretical FSM for the subsystems considered (Figure 6 and Figure 7) is presented in Table 1. In the latter, the sensitivity of each residual to each fault is detailed by means of a 0 (i.e. non-sensitive) or a 1 (i.e. sensitive) in the corresponding element of the matrix, obtaining a fault signature from each of its columns. Also, ordinal index i is assigned for each tank subsystem as follows: $i = 1$ for d175LOR, $i = 2$ for d200CGY, $i = 3$ for d268CGY and $i = 4$ for d361CGY tank subsystem. Moreover, it may be also observed how spatial consistency residuals are used for fault detection here, since $r_{i,1}$ is sensitive to all the considered faults within each i single tank subsystem, whilst TS residuals are employed for fault isolation purposes.

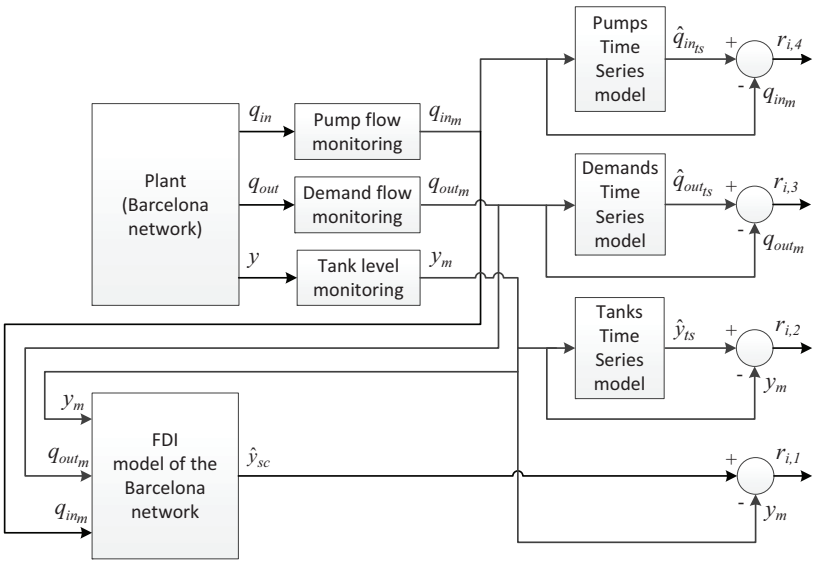

Figure 8: FDI Scheme for Barcelona DWTN

The resulting PTPR fault diagnosis scheme implemented in the Barcelona DWTN system, involving the different elements detailed in this section, is shown in Figure 8.

4.2. Fault scenarios

The Barcelona DWTN simulator allows the introduction of faults of different kinds in distinct elements of this water network. Here, faults of freezing, offset and drift nature are considered

- **Freezing:** $\Gamma(k) = 0$ and $\chi(k) = \kappa$ for $k \geq k_f$
- **Offset:** $\Gamma(k) = 1$ and $\chi(k) = \eta$ for $k \geq k_f$
- **Drift:** $\Gamma(k) = 1$ and $\chi(k) = R\left(k - k_f\right)$ for $k \geq k_f$

where κ and η are constants, R denotes the ramp function of a certain slope and k_f is the time instant when the fault is occurring.

Moreover, the faults considered are either of abrupt or incipient nature, as defined by their time profile $\beta(k)$ as follows

- **Abrupt**:

$$\beta(t) = \begin{cases} 0, & k < k_f \\ 1, & k \geq k_f \end{cases}$$

- **Incipient**:

$$\beta(t) = \begin{cases} 0, & k < k_f \\ 1 - e^{-\rho(k-k_f)}, & k \geq k_f \end{cases}$$

where $\rho > 0$ is the constant characterizing the evolution of the corresponding fault and k_f is the time instant when the fault occurs.

Different fault scenarios are defined in order to test and compare the methods presented here, all including random normally distributed measurement noise of ±1 % full scale. The dataset considered to implement these fault scenarios lasts for seven months, with a sampling period $T = 1$ hour and a fault appearing at $t_f = 744 \cdot T$ in different elements of the Barcelona DWTN subsystems considered (Figures 6 and 7, respectively):

- iOrioles pump sensor ($f_{q_{in_m}}$) in Orioles subsystem
- c175LOR demand sensor ($f_{q_{out_m}}$) in Orioles subsystem
- iCanGuey1d2 pump sensor ($f_{q_{in_{m_1}}}$) in Can Guey subsystem
- iCanGuey2 pump sensor ($f_{q_{in_{m_2}}}$) in Can Guey subsystem
- iCanGuey3 pump sensor ($f_{q_{in_{m_3}}}$) in Can Guey subsystem
- c361CGY demand sensor ($f_{q_{out_{m_2}}}$) in Can Guey subsystem
- c268CGY demand sensor ($f_{q_{out_{m_3}}}$) in Can Guey subsystem

These fault scenarios are part of a fault benchmark used in the framework of the Seventh Framework Program European project iSense (ref. FP7-ICT-2009-6) as a collaborative dataset provided by the Polytechnic University of Catalonia to be used by all the partners involved. The parametrization of the faults involved in this benchmark is depicted in Table 2.

4.3. Methods Setting

The HMM-based CDT uses ARX linear models for the extraction of the parameters θ. In the case of Orioles subsystem (Figure 6), the relationship pattern among the measured tank level, the input flow and the measured demands are modelled. The dependency graph is learned by considering all the binary relationships with autocorrelation greater or equal to $\xi_{\min} = 0.5$. The result is the graph presented in Figure 5 with $(x_1, x_2, x_3) = (y_m, q_{in_m}, q_{out_m})$. In the case of Can Guey subsystem (Figure 7), we only considered those relationships compatible with the causality given by the water flow phenomenon (i.e. those in Figure 3(a)) and selected those having autocorrelation greater or equal to $\xi_{\min} = 0.8$, where the higher threshold is due to the increased complexity of the network. Under faulty conditions, the considered relationships will exhibit changes that will depend on the kind and magnitude of the fault introduced, thus its monitoring is useful for fault isolation purposes.

Regarding the PTPR initialisation, the first 13 days of data are used as training dataset to identify the model parameters, the next 13 days are used as validation dataset to obtain the corresponding fault detection threshold and the rest of the data is used as test dataset. Regarding the HMMs, also a total of 26 days are used for training and validation purposes: 23 and 25 days were used for training the Orioles and the Can Guey cases, respectively, while the remaining days have been used to compute the threshold for detection and validation (Alippi et al., 2013). The orders of ARX models have been chosen by means of a validation procedure. The log-likelihood window length has been set to $\omega = 10$ and the batch size has been set to $N_T = 96$ and $N_T = 100$ for the Orioles and Can Guey subsystems, respectively.

4.4. Figures of Merit

The numerical results are presented by means of different figures of merit. First stage in fault diagnosis deals with faultless vs. faulty situation discrimination. The performance achieved in this fault detection stage is measured by the next indices:

- **Detection delay:** Number of samples needed by the fault diagnosis method to detect a certain fault.

- **False Positives (FP):** Percentage of test dataset faultless samples (i.e. non-affected by a certain fault) that are determined as faulty by the fault detection method.

- **False Negatives (FN):** Percentage of test dataset faulty samples (i.e. affected by a certain fault) that are determined as faultless by the fault detection method within the 72 samples (i.e. 3 days) after a fault is produced.

Moreover, the second stage in fault diagnosis involves fault isolation and classification abilities of the FDI method. These may be quantified by different figures of merit, which are defined as follows:

- **Isolation delay:** Number of samples needed by the fault diagnosis method to isolate a certain fault.

- **Isolation index:** Percentage of test dataset faulty samples (i.e. affected by a certain fault) that are properly isolated within the 72 samples (i.e. 3 days) after a fault is produced, considering a certain fault scenario.

4.5. Results

In Table 2, fault diagnosis results achieved by both FDI methods are detailed. In Figures 9 and 10, isolation results obtained by PTPR method for faults Id. 2 and Id. 14 in Table 2 are also depicted. As may be seen in the latter figures, residuals evolution fit the fault signatures corresponding to the respective faults occurring in the system when these results are attained, i.e. iOrioles actuator sensor fault ($f_{q_{in_m}}$ in Table 1) and c175LOR demand sensor fault ($f_{q_{out_m}}$ in Table 1). Similar isolation results have been obtained for faults included in Table 2 affecting similar network elements.

On the one hand, Table 2 shows generally better detection and isolation delay results achieved by PTPR method than by CFDS method, for the pump sensors of iOrioles (e.g. fault Id. 3, 4), iCanGuey1d2 (e.g. fault Id. 21, 22, 26), iCanGuey3 (e.g. fault Id. 37, 38) and the demand sensor c175LOR (e.g. fault Id. 11, 12, 13, 15, 19), with the exceptions of some faults with similar or better performance achieved by CFDS affecting iOrioles pump sensor (e.g. fault Id. 1, 2, 5, 6, 8), c175LOR (e.g. fault Id. 10),

Table 2: Faults parametrization and diagnosis results (MFD stands for maximum flow/demand)

Id.	Type of fault	Magnitude	PTPR method					CFDS method				
			Delay [# of samples]		FP [%]	FN [%]	Iso. [%]	Delay [# of samples]		FP [%]	FN [%]	Iso. [%]
			detection	isolation				detection	isolation			
1	Offset abr. iOrioles	10 % MFD	2	4	0	7.34	22.22	4	4	7.44	94.52	5.48
2	Offset abr. iOrioles	25 % MFD	2	2	0	2.37	79.16	3	3	11.57	4.11	95.89
3	Offset inc. iOrioles	10 % MFD	12	23	0	3.04	4.16	35	35	12.40	82.19	17.81
4	Offset inc. iOrioles	25 % MFD	9	13	0	4.53	52.77	16	16	0.00	27.40	72.60
5	Drift abr. iOrioles	1 % MFD	9	13	0	2.71	73.61	8	8	13.22	10.96	89.04
6	Drift abr. iOrioles	10 % MFD	3	3	0	2.78	84.72	4	4	1.65	5.48	94.52
7	Drift inc. iOrioles	1 % MFD	12	23	0	3.54	59.72	18	18	9.92	24.66	75.34
8	Drift inc. iOrioles	10 % MFD	7	7	0	4.09	77.77	4	4	8.26	8.22	91.78
9	Offset abr. c175LOR	10 % MFD	1	3	0	0.02	65.27	3	3	0.00	4.11	95.89
10	Offset abr. c175LOR	25 % MFD	1	3	0	0.02	65.27	1	1	0.00	1.37	98.63
11	Offset inc. c175LOR	10 % MFD	10	21	0	0.29	34.72	47	47	0.00	64.38	35.62
12	Offset inc. c175LOR	25 % MFD	7	11	0	0.13	58.33	65	65	0.00	89.04	10.96
13	Drift abr. c175LOR	1 % MFD	7	7	0	0.11	59.72	33	33	0.00	45.21	54.79
14	Drift abr. c175LOR	10 % MFD	2	4	0	0.04	63.88	4	4	0.00	5.48	94.52
15	Drift inc. c175LOR	1 % MFD	10	15	0	0.25	52.77	39	39	0.00	53.42	46.58
16	Drift inc. c175LOR	10 % MFD	5	7	0	0.11	59.72	8	8	38.02	10.96	89.04
17	Freezing abr. iOrioles	-	7	12	0	7.22	8.33	17	17	10.74	68.49	31.51
18	Freezing inc. iOrioles	-	19	36	0	7.52	5.55	3	3	22.31	73.97	26.03
19	Freezing abr. c175LOR	-	11	14	0	16.79	6.94	33	33	0.00	45.21	54.79
20	Freezing inc. c175LOR	-	59	-	0	92.84	0	58	58	4.13	79.45	20.55
21	Offset abr. iCanGuey1d2	15 % MFD	2	4	0	1.37	39.73	21	22	0	30.56	69.44
22	Offset inc. iCanGuey1d2	15 % MFD	9	26	0	12.33	8.22	32	50	0	69.44	30.56
23	Drift abr. iCanGuey1d2	15 % MFD	3	4	0	2.74	93.15	5	11	0	15.28	84.72
24	Freezing abr. iCanGuey1d2	-	3	8	0	9.59	71.23	12	21	0	29.17	70.83
25	Offset abr. iCanGuey2	15 % MFD	2	-	0	1.37	-	14	29	0	40.28	59.72
26	Offset inc. iCanGuey2	15 % MFD	8	26	0	12.33	2.74	32	53	0	73.61	26.39
27	Drift abr. iCanGuey2	15 % MFD	3	4	0	2.74	93.15	7	9	0	12.50	87.50
28	Freezing abr. iCanGuey2	-	3	4	0	5.48	67.12	11	12	0	16.67	83.33
29	Offset abr. c361CGY	15 % MFD	2	4	0	1.37	93.15	3	3	0	4.17	95.83
30	Offset inc. c361CGY	15 % MFD	9	11	0	10.96	82.19	10	12	0	16.67	83.33
31	Drift abr. c361CGY	15 % MFD	3	4	0	2.74	93.15	3	3	0	4.17	95.83
32	Freezing abr. c361CGY	-	10	12	0	34.25	10.96	9	11	0	15.28	84.72
33	Offset abr. c268CGY	15 % MFD	2	4	0	1.37	93.15	1	1	0	1.39	98.61
34	Offset inc. c268CGY	15 % MFD	8	11	0	9.59	80.82	3	9	0	12.50	87.50
35	Drift abr. c268CGY	15 % MFD	3	4	0	2.74	93.15	2	2	0	2.78	97.22
36	Freezing abr. c268CGY	-	10	12	0	56.16	6.85	3	11	0	15.28	84.72
37	Offset abr. iCanGuey3	15 % MFD	2	4	0	1.37	63.01	5	7	0	9.72	90.28
38	Offset inc. iCanGuey3	15 % MFD	8	28	0	28.77	12.33	28	29	0	40.28	59.72
39	Drift abr. iCanGuey3	15 % MFD	3	4	0	2.74	93.15	4	4	0	5.56	94.44
40	Freezing abr. iCanGuey3	-	3	10	0	26.03	64.38	9	13	0	18.06	81.94

c268CGY and c361CGY demand sensors (e.g. fault Id. 29 to 36), freezing incipient faults affecting Orioles system (e.g. faults Id. 18, 20) or iCanGuey pump sensor (fault Id. 25) for isolation delay. Also, generally better FP and FN rates are achieved by the PTPR method, with some exceptions regarding freezing nature faults (i.e. faults Id. 20, 32, 36, 40) for FN rates. This overall detection and isolation behavior leads to a generally quicker and more reliable diagnosis of the faulty component under study achieved by the PTPR method. On the other hand, CFDS method grants better isolation rates in general (with the exception of faults Id. 1, 12, 13, 15, 23, 24, 27 where PTPR method provides similar or better results, depending on the scenario considered) which makes it useful to confirm the isolated fault occurring in the system. It is worth noting that the CFDS method provides the performance in Table 2 without assuming any *a-priori* information about the physical model of the system. In the case of faults with an increasing profile, the detection delays of the CFDS are worse than those obtained with the PTPR method. This is due to the fact that the HMM-based CDT is more sensitive to abrupt changes in the parameter distribution. Also, CFDS is generally characterized by higher FP index values. The reason of this behaviour is twofold: nominal state approximation and process time invariance. First, the nominal model is estimated during an initial training phase that, in principle, could led to inaccurate models, i.e., model bias due to e.g. an incorrect selection of the family of models, the lack of enough data for training or the fact that training data do not excite the whole dynamics of the process. This undesired model bias tends to induce FP detections in the testing phase. Second, the process under monitoring could be intrinsically time-varying and does not follow the Markov assumption. This leads to FP detection induced by an estimated model which is not able to fully describe the process.

4.6. Discussion

From the light of the results in Section 4.5, both FDI methods introduced present satisfactory performance for the fault scenarios considered, also showing some complementarity features which suggest possible integration in order to improve the overall fault diagnosis. Specifically, the PTPR method obtains generally lower detection and isolation delays, as well as better FP and FN rates. Hence, it is a good choice for early

reliable isolation of the faults appearing in the system, whilst the CFDS obtains generally better isolation rates, which allows to reliably confirm the fault being detected and isolated. Regarding the benefits of each method, on the one hand PTPR is based on physical models describing the normal behavior and does not require to have data from all the possible fault scenarios to perform the fault diagnosis, in contrast to the CFDS method. On the other hand, the main drawback of the PTPR approach is the deep knowledge of the model structure and parameters required to successfully apply this methodology, which is not needed by the CFDS since it is a data-based approach. These facts further motivate the integration of both methods for FDI, taking advantage of the highlights which characterize each one separately.

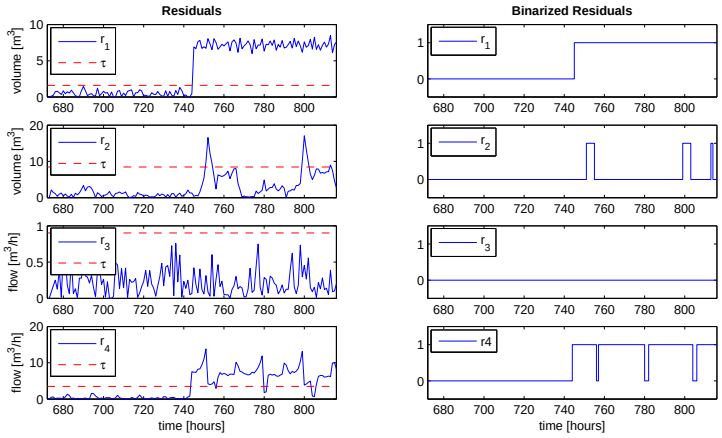

Figure 9: Fault Id.2 residuals, PTPR method

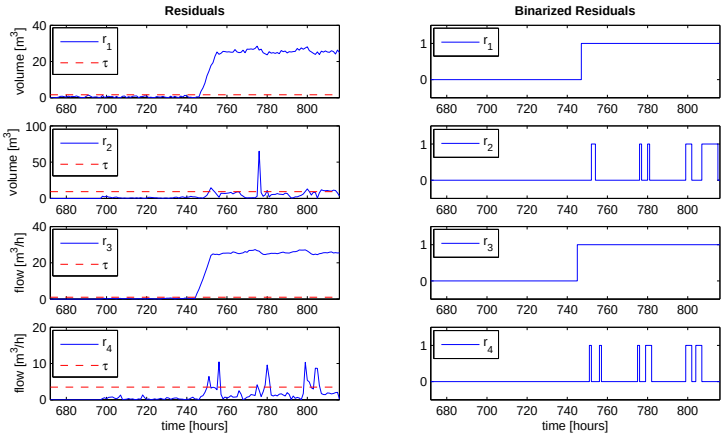

Figure 10: Fault Id.14 residuals, PTPR method

5. Conclusions

In this work, the application and comparison of two well accepted general purpose fault diagnosis methods (one model-based, the other data-based) applied to a real DWTN located in the Barcelona area, is developed. Most of the works in the literature addressing fault diagnosis in water networks have treated the problem at the distribution level, but not at the transport level. However, water transport networks have characteristics which allow the application of techniques that cannot be applied to distribution networks. The first method is built upon a model-based approach exploiting *a-priori* information regarding physical/temporal relations which exist between the measured variables within the monitored system, whilst the second aims at characterizing and detecting changes in the probabilistic pattern sequence of the data coming from this system. Some enhancements of the two approaches considered are introduced, as the use of time series residuals, not generally considered in classical residual-based fault diagnosis schemes, which traditionally use physical residuals. Successful results have been achieved by both methods, showing good complementary conditions which may suggest the integrated usage in order to improve the results achieved by each one separately. These results have been tested using heterogeneous types of faults in repre-

sentative subsystems within the network under study. Future work including additional analysis of the fault diagnosis results achieved, considering uncertainty such noise and modelling/measurement errors derived by the examination of the system under study, is to be done on the ongoing works involving the Barcelona DWTN.

Acknowledgement

This work has been partially funded by the Spanish Ministry of Science and Technology through the Project WATMAN (Ref. DPI-2009-13744), Project SHERECS (Ref. DPI-2011-26243), Project ECOCIS (Ref. DPI2013-48243-C2-1-R), Project HARCRICS (Ref. DPI2014-58104-R), and by i-Sense grant FP7-ICT-2009-6-270428 and EFFINET grant FP7-ICT-2012-318556 of the European Commission.

References

Alippi C, Ntalampiras S, Roveri M. An HMM-based change detection method for intelligent embedded sensors. In: Neural Networks (IJCNN), The 2012 International Joint Conference on. 2012. p. 1 –7. doi:10.1109/IJCNN.2012.6252610.

Alippi C, Ntalampiras S, Roveri M. A cognitive fault diagnosis system for distributed sensor networks. IEEE Transactions on Neural Networks and Learning Systems 2013;24(8):1213 –26.

Bicik J, Kapelan Z, Makropoulos C, Savić Da. Pipe burst diagnostics using evidence theory. Journal of Hydroinformatics 2011;13(4):596. URL: http://www.iwaponline.com/jh/013/jh0130596.htm. doi:10.2166/hydro.2010.201.

Blanke M, Kinnaert M, Lunze J, Staroswiecki M, Schröder J. Diagnosis and Fault-Tolerant Control. Secaucus, NJ, USA: Springer-Verlag New York, Inc., 2006.

Casillas MV, Garza LE, Puig V. Model-based leak detection and location in water distribution networks considering an extended-horizon analysis of pressure sensitivities. Journal of Hydroinformatics 2014;In Press. URL: http://www.iwaponline.com/jh/up/jh2013019.htm. doi:10.2166/hydro.2013.019.

519 Colombo A, Karney B. Energy and costs of leaky pipes: Toward compre-
520 hensive picture. J Water Resour Plann Manage 2002;128(6):441–50. URL:
521 http://dx.doi.org/10.1061/(ASCE)0733-9496(2002)128:6(441).
522 doi:10.1061/(ASCE)0733-9496(2002)128:6(441).

523 Eliades D, Polycarpou M. A fault diagnosis and security framework for water systems.
524 IEEE Transactions on Control Systems Technology 2010;18(6):1254–65.

525 Eliades D, Polycarpou M. Leakage fault detection in district metered areas of water
526 distribution systems. Journal of Hydroinformatics 2012;In Press. doi:10.2166/
527 hydro.2012.109.

528 Farley B, Mounce S, Boxall J. Development and field validation of a burst lo-
529 calization methodology. J Water Resour Plann Manage 2012;139(6):604–13.
530 URL: http://dx.doi.org/10.1061/(ASCE)WR.1943-5452.0000290. doi:10.
531 1061/(ASCE)WR.1943-5452.0000290.

532 Filion Y, Li Z, Buchberger S. Temporal and spatial scaling of instantaneous residential
533 water demand for network analysis. In: World Environmental and Water Resources
534 Congress 2007. American Society of Civil Engineers; 2007. p. 1–10. URL: http:
535 //dx.doi.org/10.1061/40927(243)512. doi:10.1061/40927(243)512.

536 Krause A, Leskovec J, Guestrin C, VanBriesen J, Faloutsos C. Efficient
537 sensor placement optimization for securing large water distribution net-
538 works. J Water Resour Plann Manage 2008;134(6):516–26. URL:
539 http://dx.doi.org/10.1061/(ASCE)0733-9496(2008)134:6(516).
540 doi:10.1061/(ASCE)0733-9496(2008)134:6(516).

541 Lees M. Data-based mechanistic modelling and forecasting of hydrological systems.
542 Journal of Hydroinformatics 2000;:15–34URL: http://www.iwaponline.com/
543 jh/002/jh0020015.htm.

544 Ljung L. Convergence analysis of parametric identification methods. Automatic Con-
545 trol, IEEE Transactions on 1978;23(5):770–83.

Ljung L. System identification. Wiley Online Library, 1999.

Makridakis S, Wheelwright S, Hyndman R. Forecasting methods and applications. John Wiley & Sons, 1998.

Meseguer J, Puig V, Escobet T. Fault diagnosis using a timed discrete-event approach based on interval observers: application to sewer networks. IEEE Transactions on Systems Man and Cybernetics Part A: Systems and Humans 2010;40(5):900–16.

Misiunas D, Vítkovský J, Olsson G, Lambert M, Simpson a. Failure monitoring in water distribution networks. Water science and technology : a journal of the International Association on Water Pollution Research 2006;53(4-5):503–11. URL: http://www.ncbi.nlm.nih.gov/pubmed/16722103.

Mounce S, Boxall J, Machell J. Development and verification of an online artificial intelligence system for detection of bursts and other abnormal flows. J Water Resour Plann Manage 2009;136(3):309–18. URL: http://dx.doi.org/10.1061/(ASCE)WR.1943-5452.0000030. doi:10.1061/(ASCE)WR.1943-5452.0000030.

Mounce SR, Boxall JB. Implementation of an on-line artificial intelligence district meter area flow meter data analysis system for abnormality detection: a case study. Water Science & Technology: Water Supply 2010;10:437–44.

Mounce SR, Mounce RB, Boxall JB. Novelty detection for time series data analysis in water distribution systems using support vector machines. Journal of Hydroinformatics 2011;13(4):672. URL: http://www.iwaponline.com/jh/013/jh0130672.htm. doi:10.2166/hydro.2010.144.

Ostfeld A, Salomons E. Optimal layout of early warning detection stations for water distribution systems security. J Water Resour Plann Manage 2004;130(5):377–85. URL: http://dx.doi.org/10.1061/(ASCE)0733-9496(2004)130:5(377). doi:10.1061/(ASCE)0733-9496(2004)130:5(377).

Palau C, Arregui F, Carlos M. Burst detection in water networks using principal component analysis. J Water Resour Plann Manage 2011;138(1):47–54.

URL: http://dx.doi.org/10.1061/(ASCE)WR.1943-5452.0000147. doi:10.1061/(ASCE)WR.1943-5452.0000147.

Perez R, Puig V, Pascual J, Quevedo J, Landeros E, Peralta A. Methodology for leakage isolation using pressure sensitivity analysis in water distribution networks. Control Engineering Practice 2011;19(10):1157–67. URL: http://www.sciencedirect.com/science/article/pii/S0967066111001201.

Prescott SL, Ulanicki B. Time series analysis of leakage in water distribution networks. Water software systems - Theory and applications 2001;2:17–28.

Pérez R, Puig V, Pascual J, Quevedo J, Landeros E, Peralta A. Leakage isolation using pressure sensitivity analysis in water distribution networks: Application to the Barcelona case study. In: 12th IFAC Symposium on Large-Scale Systems: Theory and Applications. volume 9; 2010. p. 578–84.

Puig V, Blesa J. Limnimeter and rain gauge FDI in sewer networks using an interval parity equations based detection approach and an enhanced isolation scheme. Control Engineering Practice 2013;21(2):146–70.

Puig V, Stancu A, Escobet T, Nejjari F, Quevedo J, Patton R. Passive robust fault detection using interval observers: Application to the damadics benchmark problem. Control Engineering Practice 2006;14(6):621–33. URL: http://www.sciencedirect.com/science/article/pii/S0967066105001048.

Quevedo J, Chen H, Cugueró MA, Tino P, Puig V, García D, Sarrate R, Yao X. Combining learning in model space fault diagnosis with data validation/reconstruction: Application to the barcelona water network. Engineering Applications of Artificial Intelligence 2014;30(0):18–29. URL: http://www.sciencedirect.com/science/article/pii/S0952197614000153.

Quevedo J, Puig V, Cembrano G, Blanch J, Aguilar J, Saporta D, Benito G, Hedo M, Molina A. Validation and reconstruction of flow meter data in the Barcelona water distribution network. Control Engineering Practice

2010;18(6):640–51. URL: http://linkinghub.elsevier.com/retrieve/pii/S0967066110000791. doi:10.1016/j.conengprac.2010.03.003.

Ragot J, Maquin D. Fault measurement detection in an urban water supply network. Journal of Process Control 2006;16(9):887–902. URL: http://www.sciencedirect.com/science/article/pii/S0959152406000655. doi:10.1016/j.jprocont.2006.06.005.

Romano M, Kapelan Z, Savic D. Geostatistical techniques for approximate location of pipe burst events in water distribution systems. Journal of Hydroinformatics 2013;15(3):634–51.

Romano M, Kapelan Z, Savic D. Automated detection of pipe bursts and other events in water distribution systems. J Water Resour Plann Manage 2014a;140(4):457–67. URL: http://dx.doi.org/10.1061/(ASCE)WR.1943-5452.0000339. doi:10.1061/(ASCE)WR.1943-5452.0000339.

Romano M, Kapelan Z, Savic D. Evolutionary algorithm and expectation maximization strategies for improved detection of pipe bursts and other events in water distribution systems. J Water Resour Plann Manage 2014b;140(5):572–84. URL: http://dx.doi.org/10.1061/(ASCE)WR.1943-5452.0000347. doi:10.1061/(ASCE)WR.1943-5452.0000347.

Winters PR. Forecasting sales by exponentially weighted moving averages. Management Science 1960;6(52):324–42. URL: http://www.jstor.org/stable/10.2307/2627346.

Wu Z. Online monitoring and detection; Exton: Bentley Systems. p. 168–89.

Wu Z, Sage P, Turtle D. Pressure-dependent leak detection model and its application to a district water system. Journal of Water Resources Planning and Management 2010;136(1):116–28. URL: http://ascelibrary.org/doi/abs/10.1061/(ASCE)0733-9496(2010)136:1(116). doi:10.1061/(ASCE)0733-9496(2010)136:1(116).